Supporting Information

Low-temperature Li plating/corrosion hazard in Li ion-batteries: Electrode rippling, variable states of charge, thermal and non-thermal runaway

Benjamin Ng[a], Paul T. Coman[a], Ehsan Faegh[a], Xiong Peng[c], Stavros G. Karakalos[a], Xinfang Jin[b], William E. Mustain[a], Ralph E. White[a,*]

[a]Department of Chemical Engineering, University of South Carolina, Columbia, SC 29208, United States
[b]Department of Mechanical Engineering, University of Massachusetts, Lowell, MA 01854, United States
[c]Energy Conversion Group, Lawrence Berkeley National Laboratory, Berkeley, CA, 94720, United States

[*]Corresponding authors: William Mustain: mustainw@mailbox.sc.edu; Ralph White: white@cec.sc.edu

Keywords: Li-ion battery; NMC532; full-cell; failure; safety; thermal runaway

S1. Spatial definitions of the jellyroll

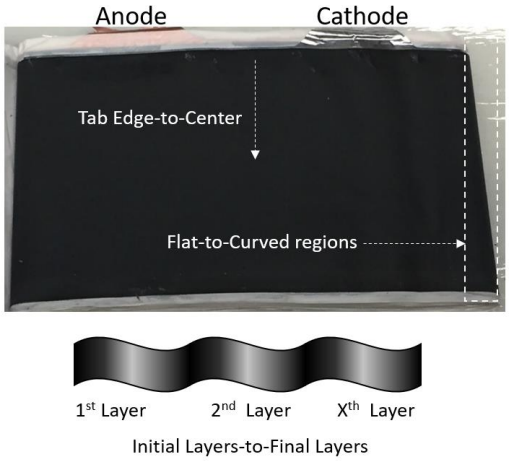

Figure S1. Defining tab edge-to-center, flat-to-curved regions, and initial layers-to-final layers in the main document.

S2. Elemental Composition: Inductively coupled plasma atomic emission spectroscopy (ICP-OES)

The ICP-OES elemental analysis was done twice by aqua regia (HNO_3 and HCl at 1:3 molar ratio) and nitric acid (HNO_3). The emission of radiation at 610.37nm (Li), 238.89nm (Co), 230.29nm (Ni), and 257.60nm (Mn) are characteristic for the element. In addition, the relative intensity can be related back to the calibration data that collects a distribution of the possible elemental content for Li, Ni, Mn, and Co. The cathode intensity was found 69595a.u., 120889a.u., 290719a.u., and 155454a.u. which corresponds to the calibration data of atomic ratios for Ni = 0.48, Mn = 0.28, and Co = 0.20. The same elemental composition was collected for the anode and confirmed negligible Co, Ni, and Mn.

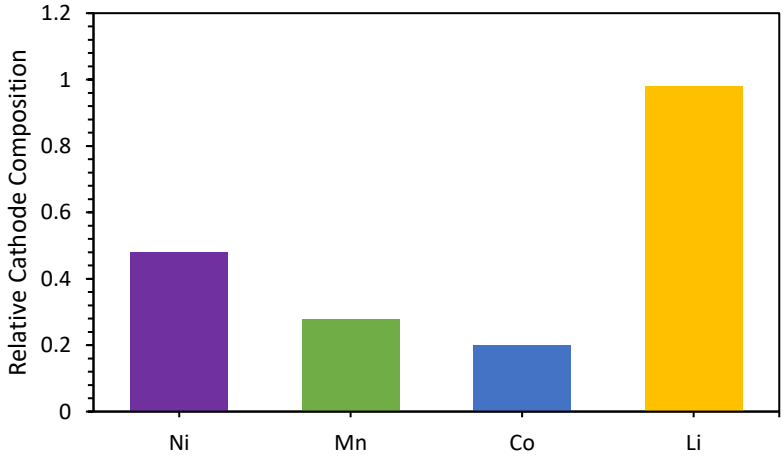

Figure S2. ICP-OES analysis of the $Li_z(Ni_bMn_cCo_d)O_2$ which indicates a = 0.98, b = 0.48, c = 0.28, d = 0.2 and consistent with NMC532 cathode chemistry.

S3. Three-electrode setup for the identification of Li^0 plating

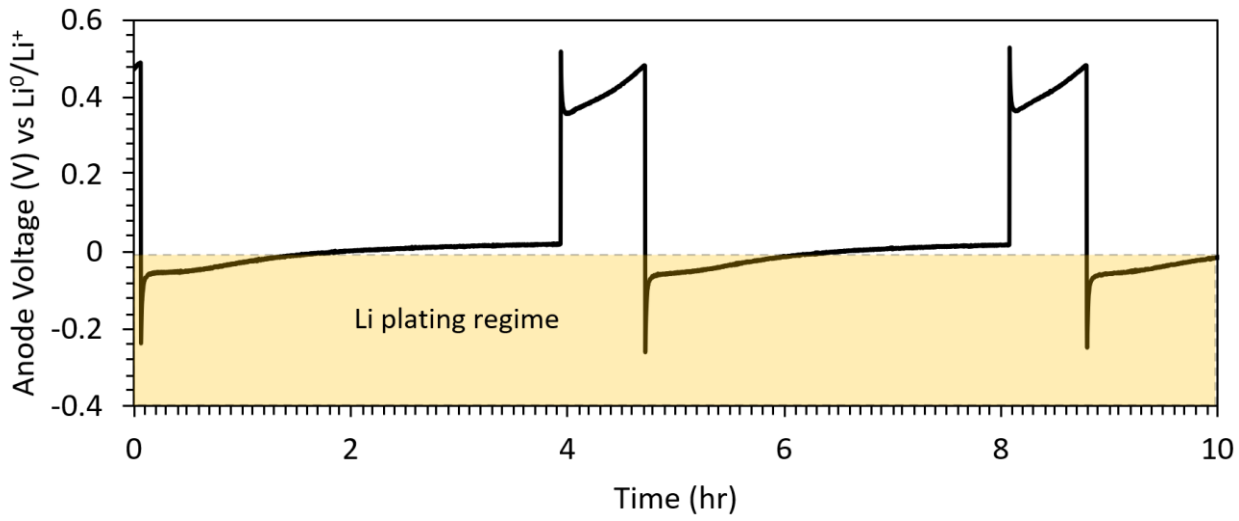

Figure S3. Depicts voltage profile vs Li^0/Li^+ at -29°C for the 3-electrode setup and indicates the high overpotentials at low temperature. The severe polarization enables severe capacity loss due to Li^0 plating and parasitic side reactions that consume charge.

S4. Spatial dependence of morphology (low temperature cycling): Li_xC_6 and $Li(Ni_{0.5}Mn_{0.3}Co_{0.2})O_2$

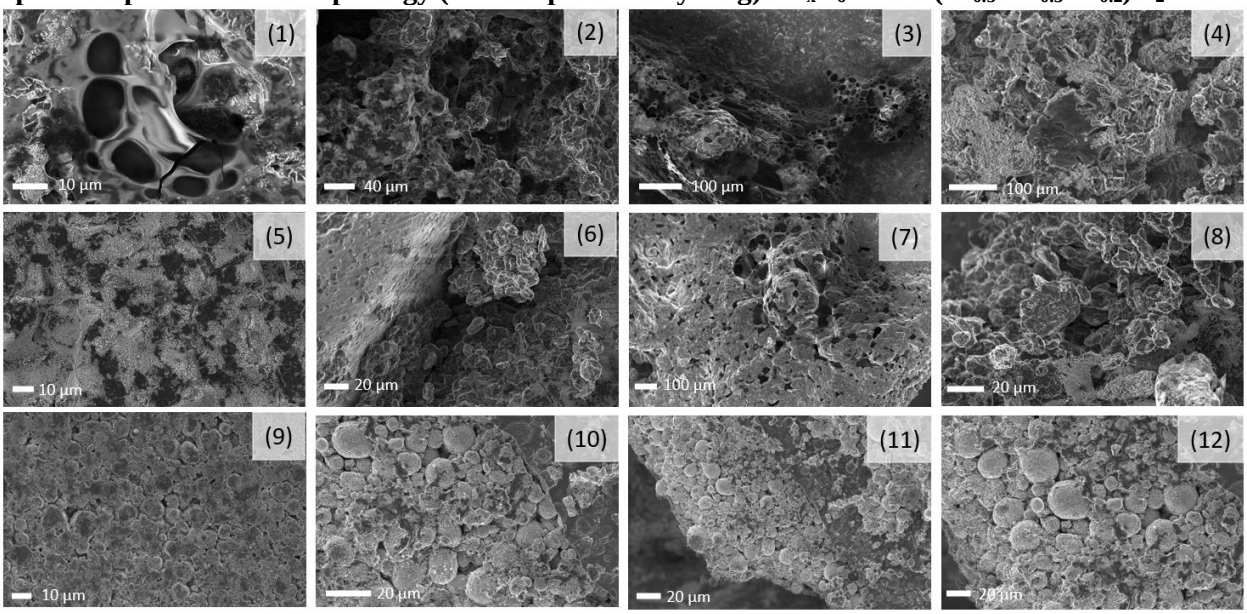

Figure S4. Field emission scanning electron microscope (FE-SEM) of the Li_xC_6 anode (1-8) and $Li(Ni_{0.5}Mn_{0.3}Co_{0.2})O_2$ cathode (9-12). The regions of the electrodes follow the same designation as that in the main document.

S5. Theoretical calculations for the state of lithiation based on A_{1g}/E_g ratios from Raman spectroscopy

Calibration data for Raman spectroscopy was done to extrapolate the state of lithiation for the post-mortem electrodes. Pristine electrodes were cycled at various points to determine the A_{1g}/E_g ratios. Based on the calibration data, the theoretical state of lithiation was determined for different electrode regions.

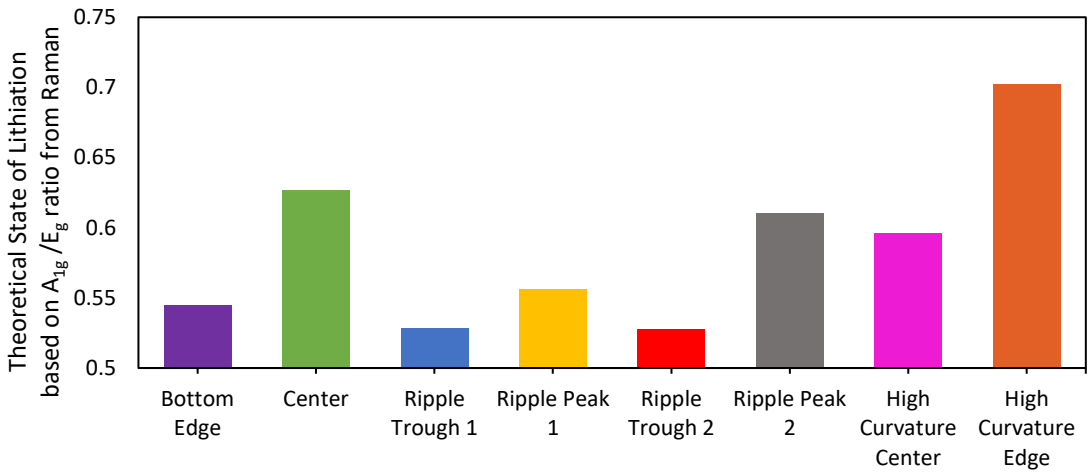

Figure S5. Raman spectroscopy analysis and correlation to calibration data to extrapolated the state of lithiation by A_{1g}/E_g peak ratio. Note: this calculation is an estimate and does not take inconsideration of spectrum changes due to cathode degradation

S6. Reaction mechanism for Gas formation and Li-carbide

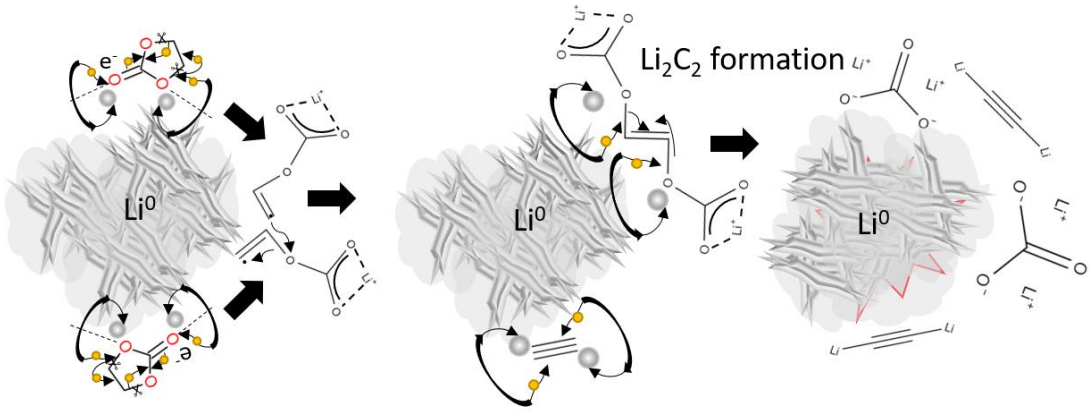

Figure S6. Li_2C_2 reaction pathway from Li^0 corrosion. Wang et al.[1] calculated a Gibb's free energy of reduction and ring-opened Li^+-EC of ΔG=- 101.25 kJ/mol and the intermediate can further minimize the free energy by dimerization and releasing an adsorbed acetylene (ΔG = -281.165 kJ/mol). The dimerization product, lithium vinylene dicarbonate,can further decompose via Li^0 corrosion and produce Li_2C_2.

S7. Spatially dependent chemistry: X-ray photoelectron spectroscopy (XPS

S7.1 Background X-ray photoelectron spectroscopy (XPS) of pristine $Li(Ni_{0.5}Mn_{0.3}Co_{0.2})O_2$

The wide spectrum XPS scan shows the presence Co, Ni, Mn F, O, C, and Li. The transition metal oxides that makes NMC532 consist of a Co2p spectrum that shows the presence of CoO at the peak of 780.2eV, a Ni2p peak at 854.9eV for NiO, and Mn2p peak at 642.5eV for MnO_2. There the oxidation states of Co is in the 2+ state, Ni is in the 2+ state, and Mn is in the +4 state. No additional peaks were observed that can be ascribed to contaminants or other oxidation states of Ni, Co, and Mn. The Li1s spectrum indicates the presence for Li_2O_2 at 54.1eV and LiF at 55.2eV. Additional C, O and F elements come from the binder and conductive carbon.

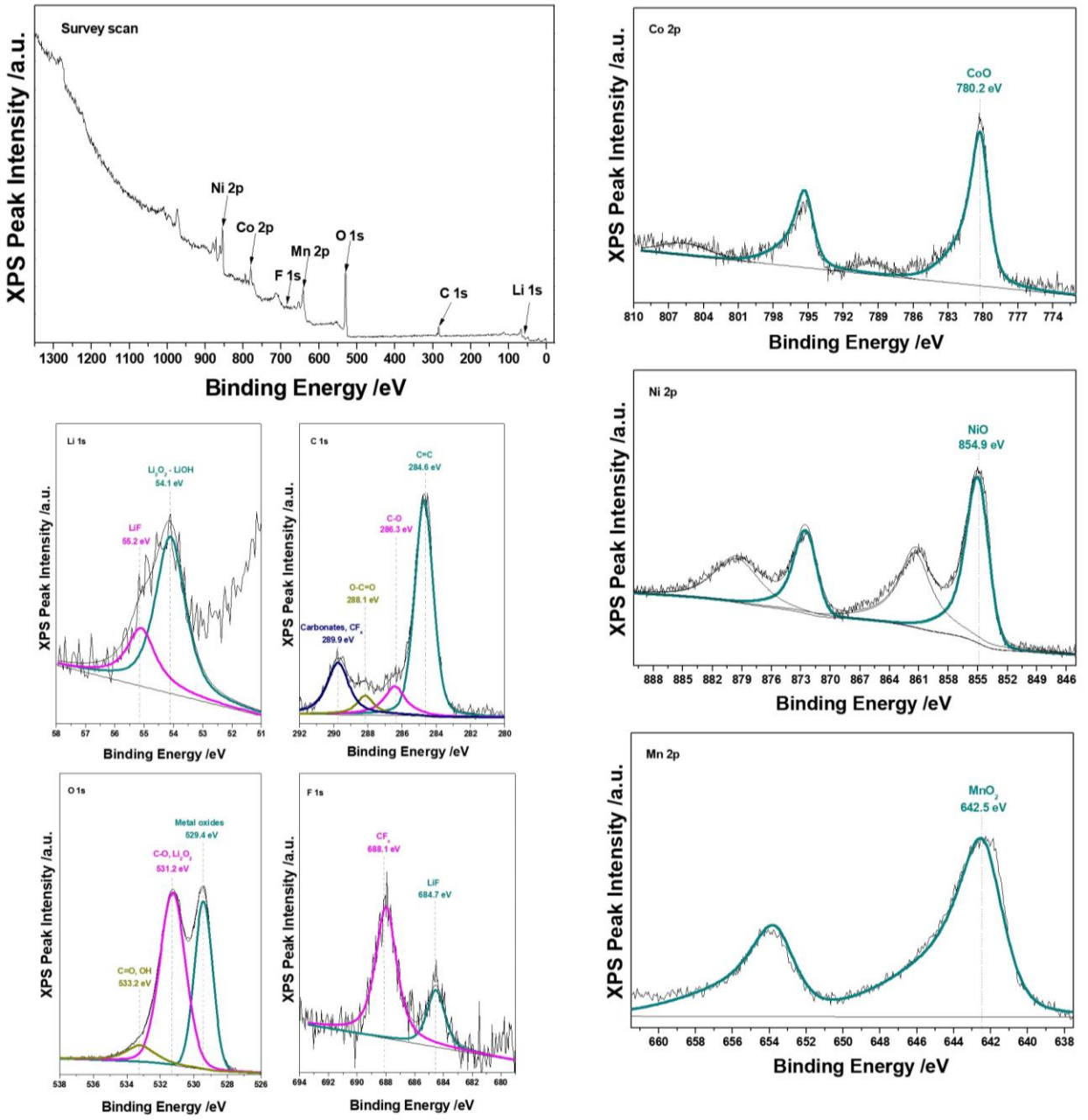

Figure S7 X-ray photoelectron spectroscopy (XPS) deconvolution of the surface species of pristine NMC532

S7.2 Normal cycled $Li(Ni_{0.5}Mn_{0.3}Co_{0.2})O_2$ and spatially distributed surface chemistry

Determining the electrolyte decomposition products for normally cycled NMC532 is an extensive task that requires significant analysis and backtracking. The most well-known surface analysis technique is X-ray Photoelectron Spectroscopy (XPS). Prior to XPS, each electrode was rinsed in DMC for 15 minutes to remove residual salt deposits. The electrodes were cut into 1.76 cm^2 disk electrodes for XPS.

Table S1 . Represents the mass/atomic spatial distribution (edge, center, curved) region for NMC532 after normal cycling

Edge	Li	C	O	Mn	F	Co	Ni
Mass Conc. %	5.5	25.5	20.5	5.8	23.9	3.1	14.8
Atomic Conc. %	13.5	36.0	21.7	1.7	21.3	0.9	4.2

Center	Li	C	O	Mn	F	Co	Ni
Mass Conc. %	7.0	22.1	22.0	5.7	24.1	3.9	14.7
Atomic Conc. %	17.0	30.9	23.2	1.7	21.3	1.1	4.2

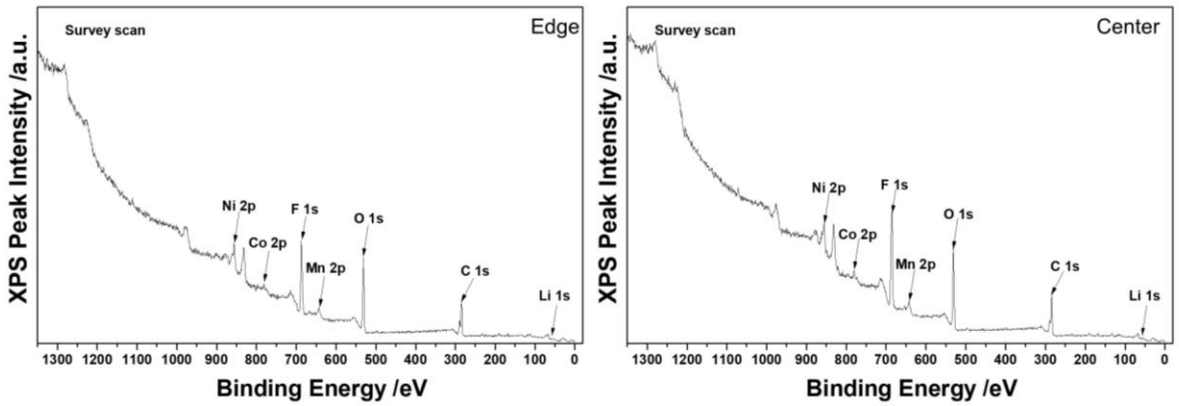

Figure S8 XPS wide scan spectrum for NMC532 and spatially distributed surface chemistry (e.g. edge, center) after normal cycling.

The binding energy for Co, Mn, and Ni at 780.2eV, 642.4eV, and 855.7eV which correspond to Co^{2+}, Mn^{4+}, and Ni^{3+} respectively. Normally cycled NMC532 consist of MnO_2 and MnF_x for manganese species, CoO and $Co(OH)_2$ for cobalt species, and Ni_2O_3 for nickel species. Co 2p spectrum exhibits 2 define peaks: $2p_{3/2}$ (780.2eV), $2p_{1/2}$(795.0 eV) indicating a spin orbital splitting of ~15.0eV. Trace Co^{4+} was detected at weak peaks 782.1 and 796.6 eV. Mn 2p spectrum shows 2 define peaks: $2p_{3/2}$ (642.5eV), $2p_{1/2}$ (654.5eV) with a separation of ~12eV, which correspond to Mn^{4+} cation. Ni 2p spectrum has 2 dominant peaks: $2p_{3/2}$ (854.4 eV) and $2p_{1/2}$ (872.3eV) indicating presence of Ni^{2+}. Peaks 856.5, 863.9, 874, and 882.4 eV indicates the existence of higher oxidation states of Ni^{3+}. Good amount of NiF_x in cycled cathodes. Possibly rules out **only** VC-additive due to typical poly(VC)-dominance in CEI over NiF_x.

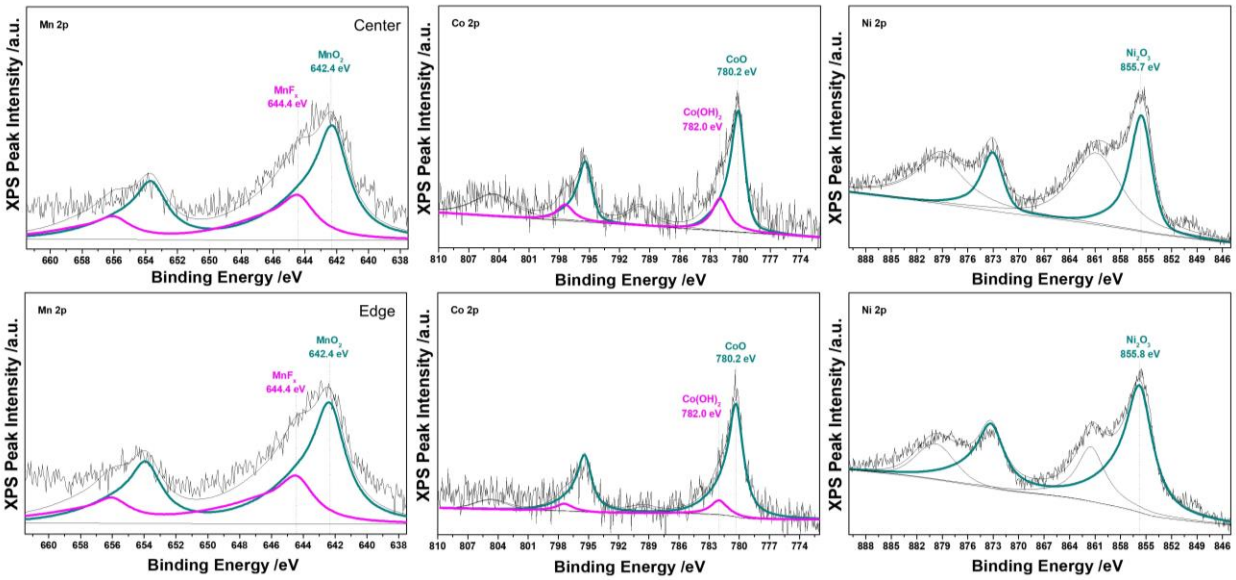

Figure S9 XPS Mn2p, Co2p, and Ni2p spectrum for NMC532 and spatially distributed surface chemistry (e.g. edge, center) after normal cycling

The C1s peak contains C-O, C=O, -CO_2- and -CO_3- functionalities. The F1s spectra displays strong peaks at 687.7 eV, which is attributed to C-F bonds from binder and 685 eV for metal fluorides (NiF_x, MnF_x, CoF_x, LiF). The O1s contains a strong peak at 531.6eV which derives C-O bonds and Li_2O_2. A weak shoulder peak at 529.7eV indicates lattice M-O bonds in NMC523 layered structure and possible loss in oxygen due to loss in intensity such as spinel-like phase change, surface structure degradation, Mn^{2+} dissolution. In addition, the broadening peak 533.2 eV indicates presence of poly(VC) and various O/F substituted $Li_xPO_yF_z$. In addition, the Li1s spectra contains LiF at spectral peak 55.5eV and Li_2O species at 54.2eV.

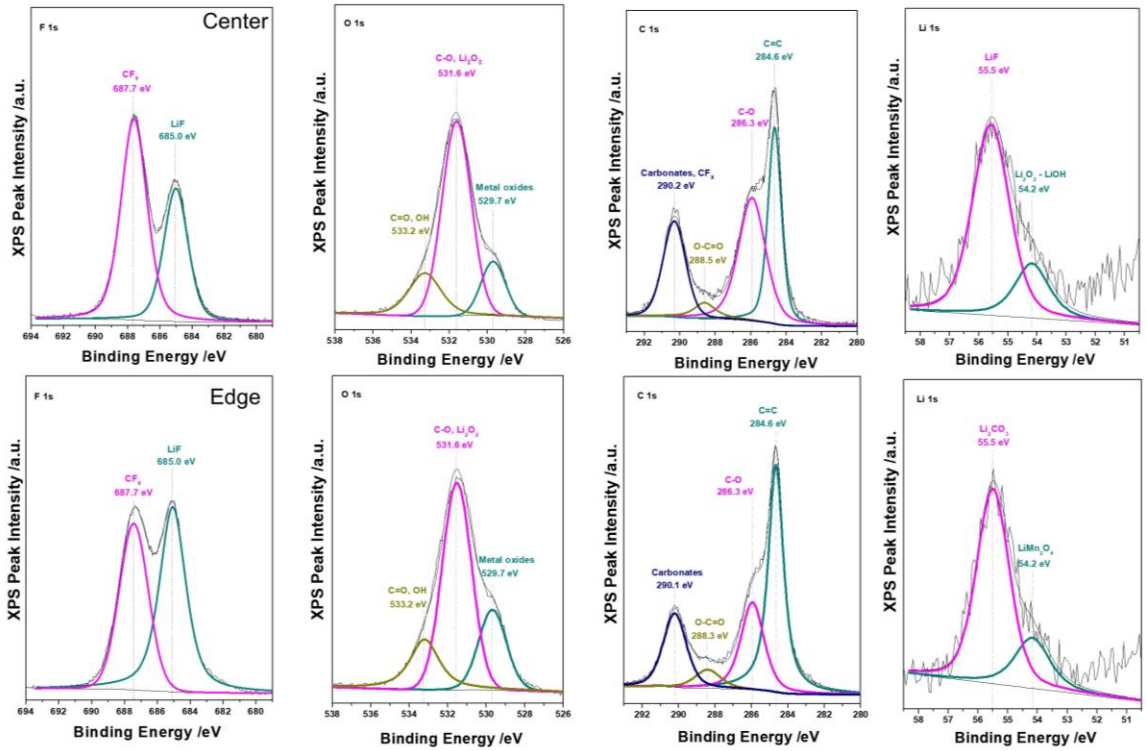

Figure S10 XPS F1s, O1s, C1s, and Li1s spectrum for NMC532 and spatially distributed surface chemistry (e.g. edge, center, curvature) after post-mortem.

S7.3 Post mortem $Li(Ni_{0.5}Mn_{0.3}Co_{0.2})O_2$ and spatially distributed surface chemistry

Table S2. Represents the mass/atomic spatial distribution (edge, center, curved) region for NMC532 and graphite after post-mortem

$Li(Ni_{0.5}Mn_{0.3}Co_{0.2})O_2$

Edge	Li	P	C	O	Mn	F	Co	Ni
Mass Conc. %	7.1	2.6	35.6	22.8	0.9	21.6	0.4	9.0
Atomic Conc. %	15.1	1.3	43.2	21.0	0.3	16.7	0.1	2.3

Center	Li	P	C	O	Mn	F	Co	Ni
Mass Conc. %	3.2	1.9	40.2	18.9	2.2	19.6	3.1	10.9
Atomic Conc. %	7.3	1.0	52.6	18.5	0.6	16.3	0.8	2.9

Curved	Li	P	C	O	Mn	F	Co	Ni
Mass Conc. %	5.1	1.2	38.0	23.2	1.0	18.4	3.3	9.8
Atomic Conc. %	11.1	0.6	48.0	22.0	0.3	14.6	0.9	2.5

Li_xC_6

Edge	Li	P	C	O	Mn	F	Ni
Mass Conc. %	16.7	1.6	26.3	38.4	0.0	13.2	3.8
Atomic Conc. %	30.8	0.7	28.0	30.8	0.0	8.9	0.8

Center	Li	P	C	O	Mn	F	Ni
Mass Conc. %	8.2	2.1	35.0	32.2	0.7	15.9	5.9
Atomic Conc. %	16.5	0.9	40.9	28.3	0.2	11.8	1.4

Curved	Li	P	C	O	Mn	F	Ni
Mass Conc. %	12.2	2.5	31.1	31.7	0.0	17.7	4.8
Atomic Conc. %	23.6	1.1	34.8	26.9	0.0	12.5	1.1

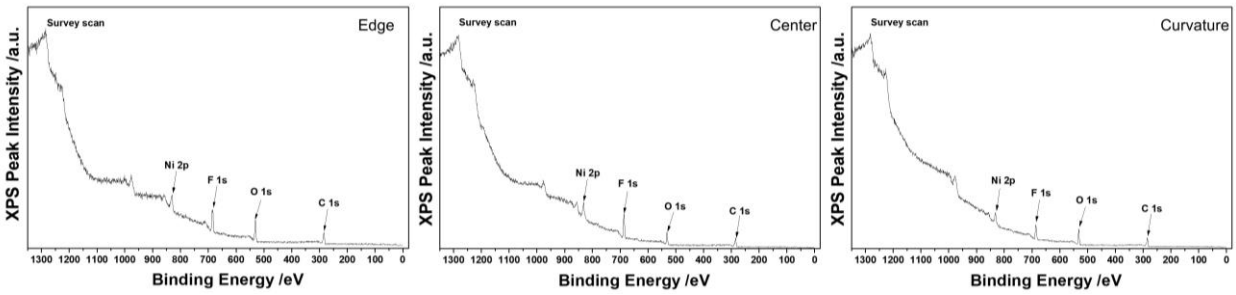

Figure S11. XPS wide scan spectrum for NMC532 and spatially distributed surface chemistry (e.g. edge, center, curvature) after post-mortem

Percentages	Edge	Center	Curvature
Mass %	35.6	40.2	38.0
Atomic %	43.2	52.6	48.0

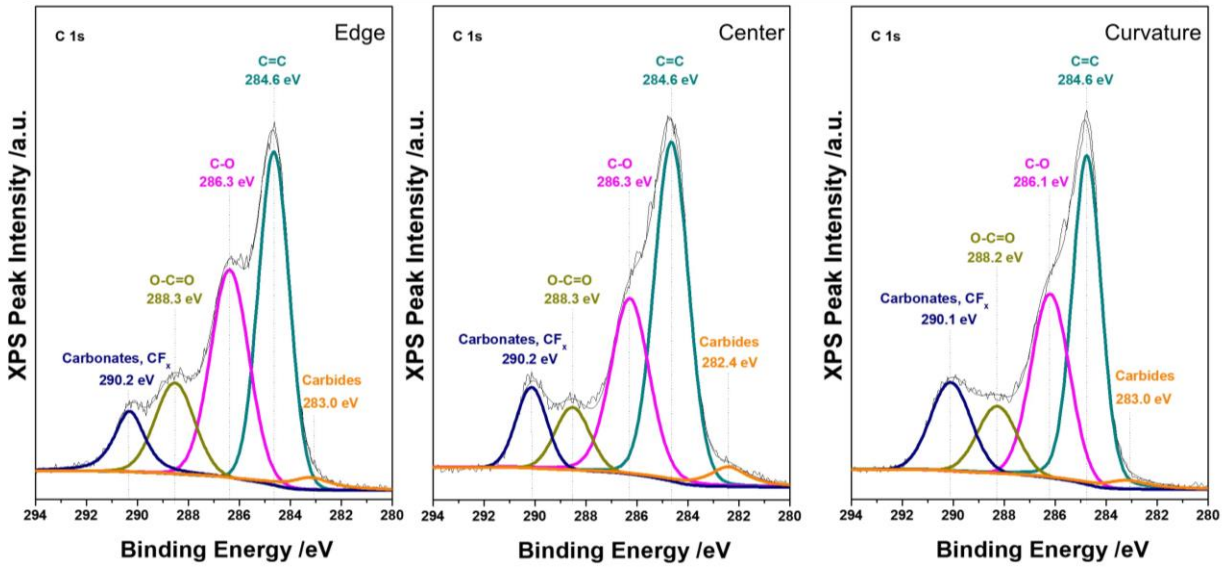

Figure S12. XPS C1s spectrum for NMC532 and spatially distributed surface chemistry (e.g. edge, center, curvature) after post-mortem.

Percentages	Edge	Center	Curvature
Mass %	7.1	3.2	5.1
Atomic %	15.1	7.3	11.1

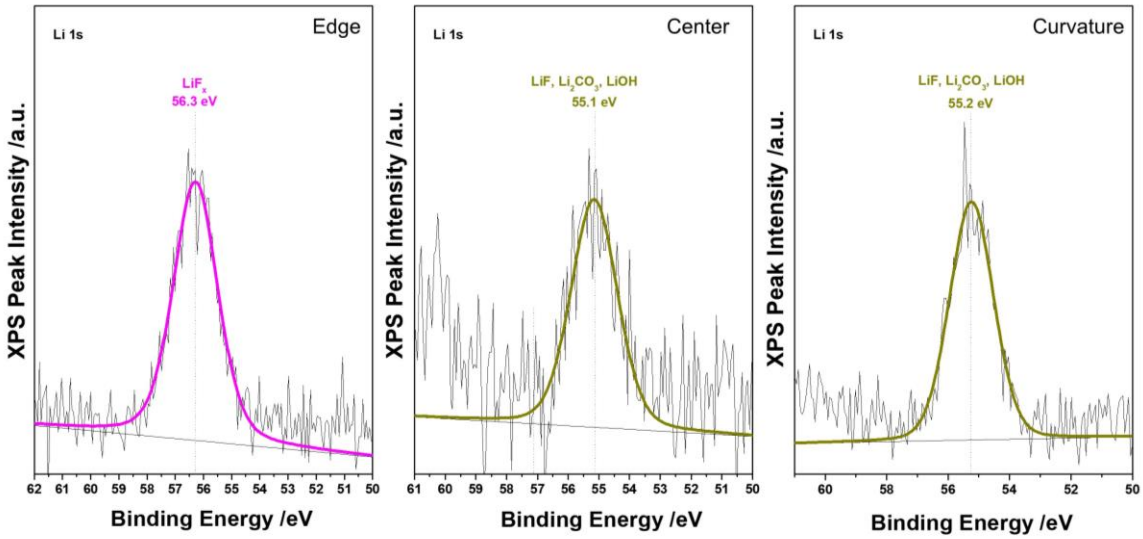

Figure S13. XPS Li1s spectrum for NMC532 and spatially distributed surface chemistry (e.g. edge, center, curvature) after post-mortem.

Percentages	Edge	Center	Curvature
Mass %	0.4	3.1	3.3
Atomic %	0.1	0.8	0.9

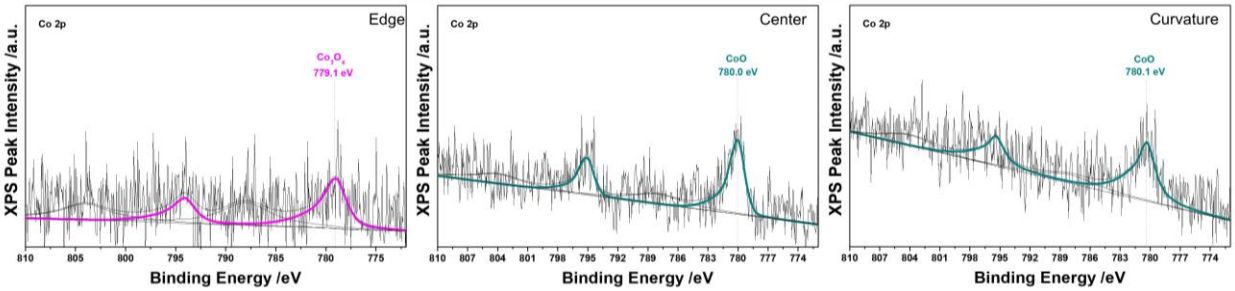

Figure S14 XPS Co2p spectrum for NMC532 and spatially distributed surface chemistry (e.g. edge, center, curvature) after post-mortem

Percentages	Edge	Center	Curvature
Mass %	9.0	10.9	9.8
Atomic %	2.3	2.9	2.5

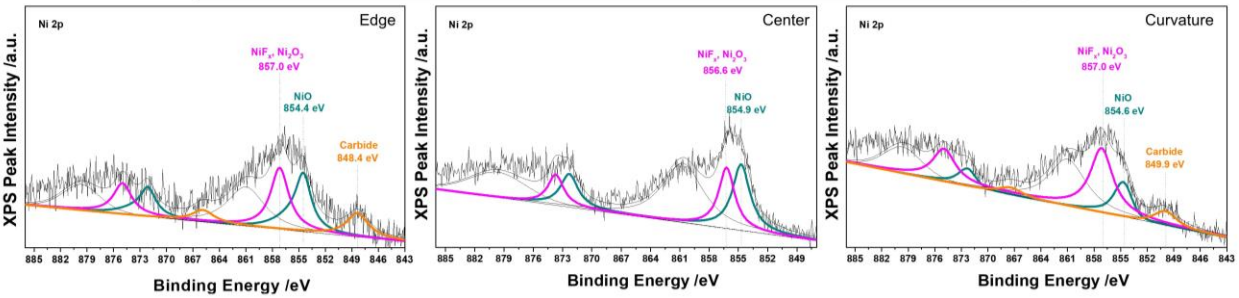

Figure S15 XPS Ni2p spectrum for NMC532 and spatially distributed surface chemistry (e.g. edge, center, curvature) after post-mortem.

Percentages	Edge	Center	Curvature
Mass %	0.9	2.2	1.0
Atomic %	0.3	0.6	0.3

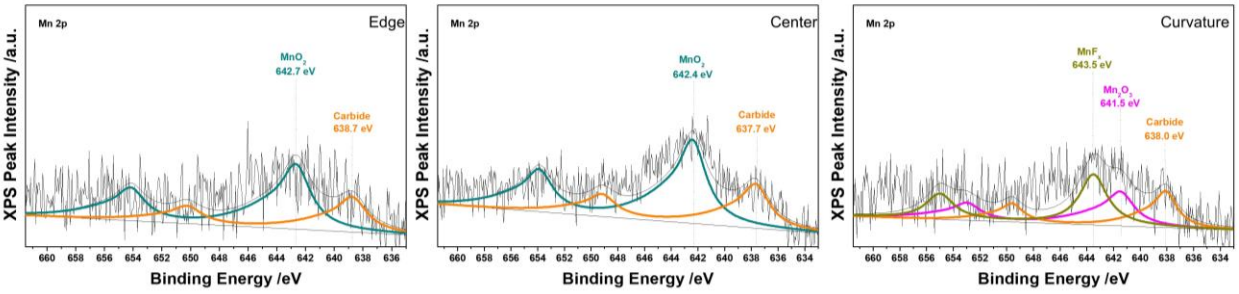

Figure S16 XPS Mn2p spectrum for NMC532 and spatially distributed surface chemistry (e.g. edge, center, curvature) after post-mortem.

Percentages	Edge	Center	Curvature
Mass %	21.6	19.6	18.4
Atomic %	16.7	16.3	14.6

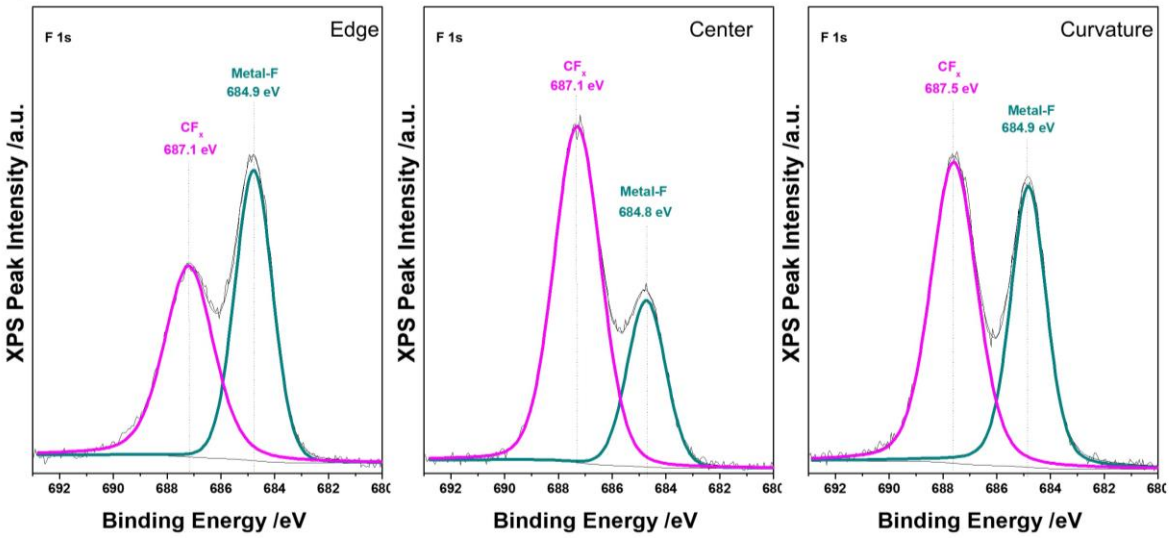

Figure S17 XPS F1s spectrum for NMC532 and spatially distributed surface chemistry (e.g. edge, center, curvature) after post-mortem

Percentages	Edge	Center	Curvature
Mass %	22.8	18.9	23.2
Atomic %	21.0	18.5	22.0

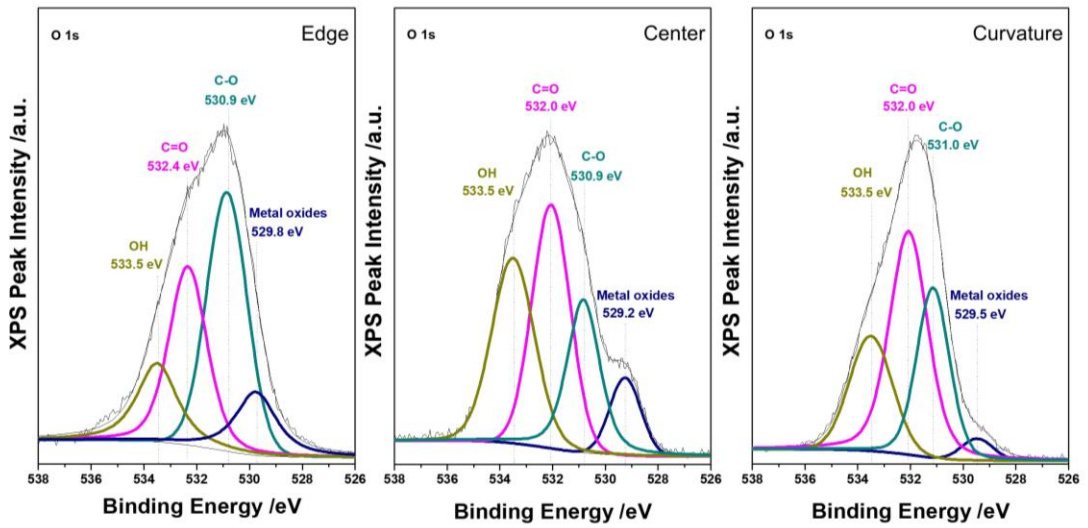

Figure S18 XPS O1s spectrum for NMC532 and spatially distributed surface chemistry (e.g. edge, center, curvature) after post-mortem.

Percentages	Edge	Center	Curvature
Mass %	2.6	1.9	1.2
Atomic %	1.3	1.0	0.6

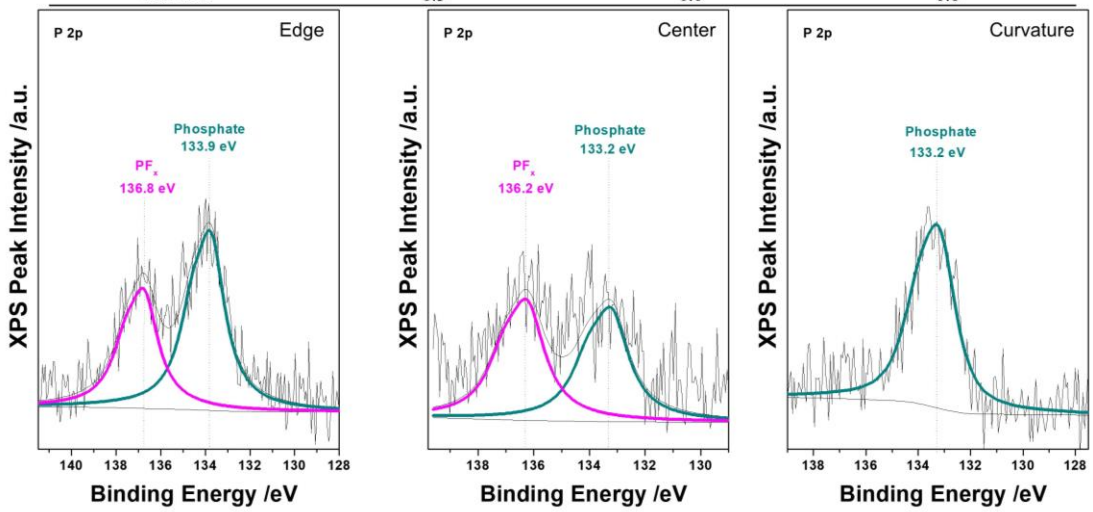

Figure S19 XPS P2p spectrum for NMC532 and spatially distributed surface chemistry (e.g. edge, center, curvature) after post-mortem.

S7.4 Normal cycled Li_xC_6 and spatially distributed surface chemistry

There are C1s spectral peaks at 284.6 eV (C=C), 285.5 eV (C-C), 286.7 eV(C-O), and 288.5 eV(O-C=O). The peaks at 284.6 and 285.5 eV corresponds to graphite. The F1s peaks at 687.0 eV and 684.4 eV correspond to C-F bond in the binder and presence of metal fluorides like LiF. Additional peaks in the O1s spectrum consist of 533.5 eV (C=O), 531.9 (C-O) and 530.4 eV $Ni(OH)_2$. The presence of Ni dissolution from the cathode was found for normally cycled cells. The Ni2p spectrum contains 859.3 eV and 856.9 eV peaks which correspond to the presence of NiF_x and $Ni(OH)_2$.

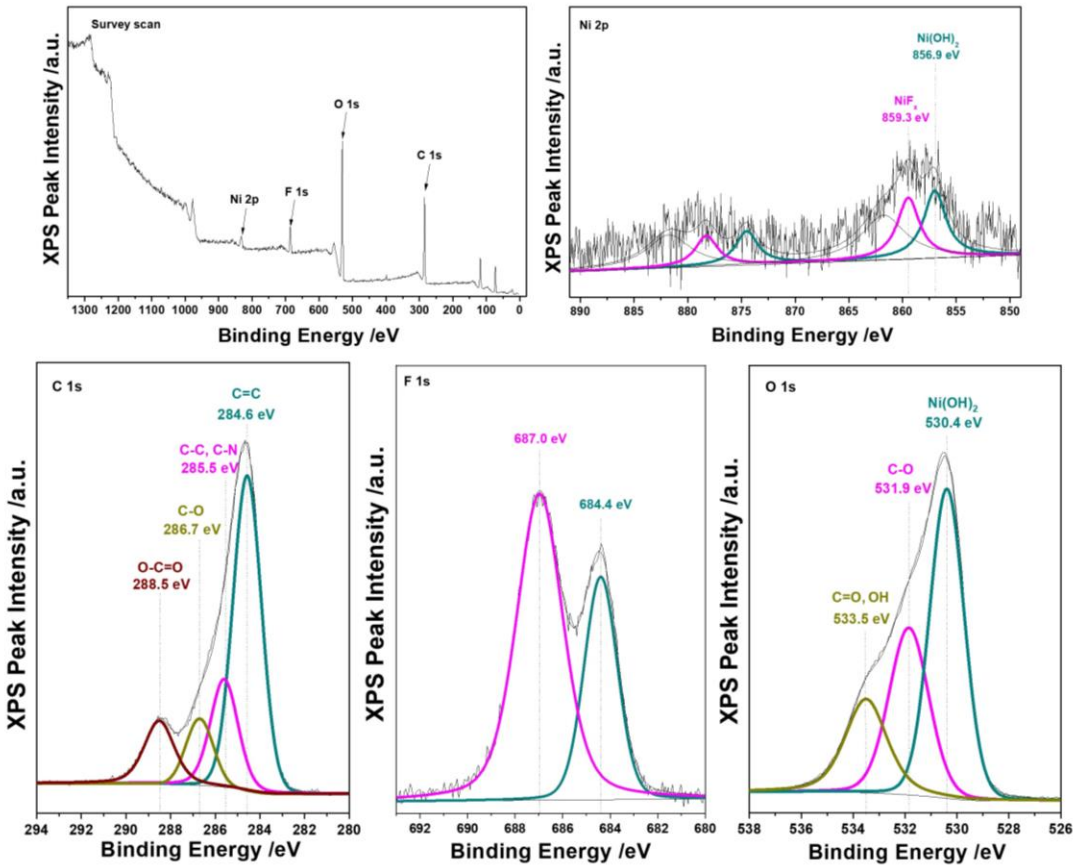

Figure S20 XPS wide scan, Ni2p, C1s, F1s, and O1s spectrum for Li_xC_6 and spatially distributed surface chemistry (e.g. edge, center, curvature) after normal cycled.

S7.5 Post-mortem Li_xC_6 and spatially distributed surface chemistry

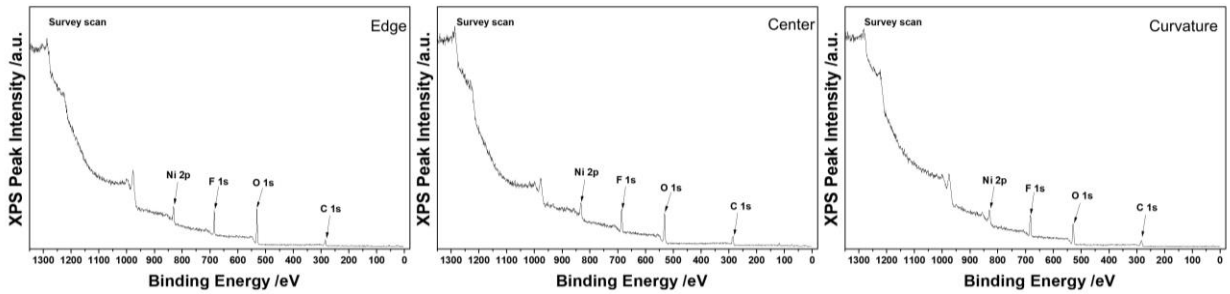

Figure S21 XPS wide scan spectrum for Li_xC_6 and spatially distributed surface chemistry (e.g. edge, center, curvature) after post-mortem

Percentages	Edge	Center	Curvature
Mass %	26.3	35.0	31.1
Atomic %	28.0	40.9	34.8

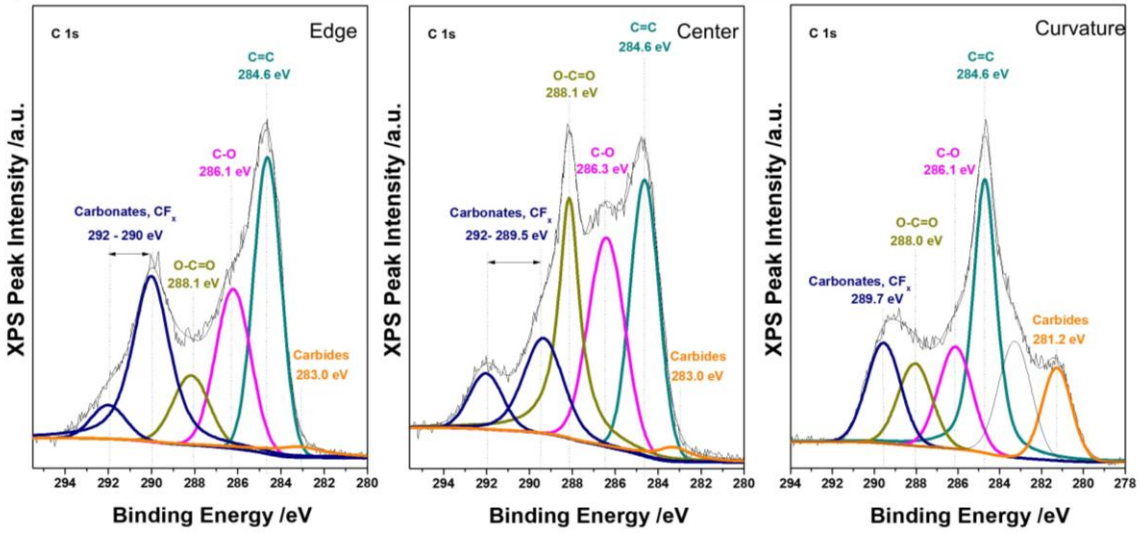

Figure S22 XPS C1s spectrum for Li_xC_6 and spatially distributed surface chemistry (e.g. edge, center, curvature) after post-mortem.

Percentages	Edge	Center	Curvature
Mass %	16.7	8.2	12.2
Atomic %	30.8	16.5	23.6

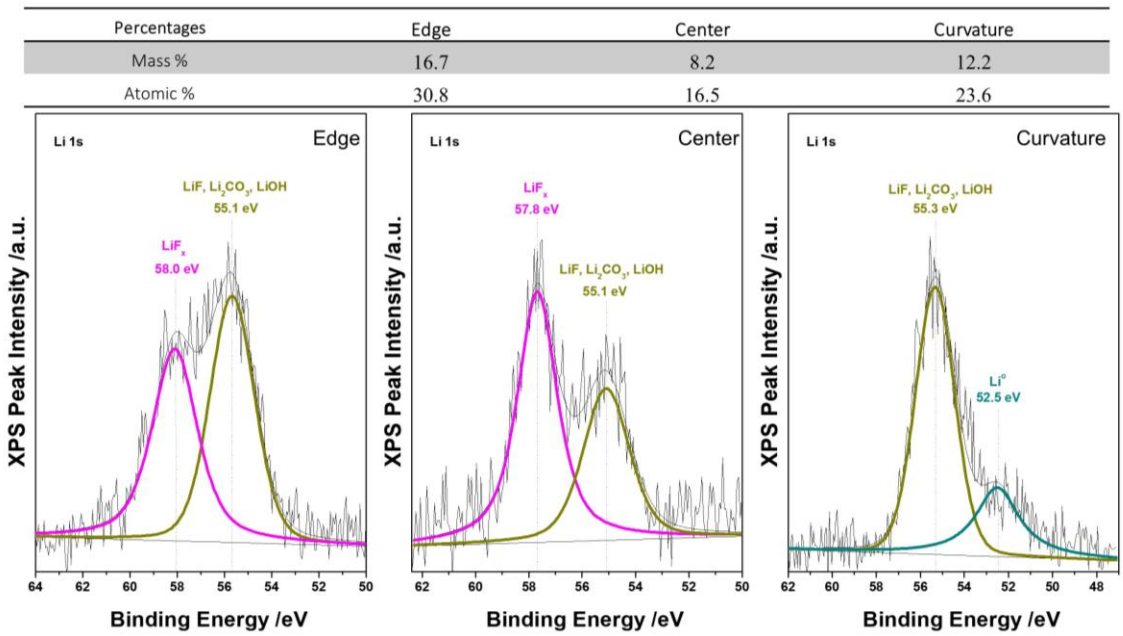

Figure S23 XPS Li1s spectrum for Li_xC_6 and spatially distributed surface chemistry (e.g. edge, center, curvature) after post-mortem.

Percentages	Edge	Center	Curvature
Mass %	3.8	5.9	4.8
Atomic %	0.8	1.4	1.1

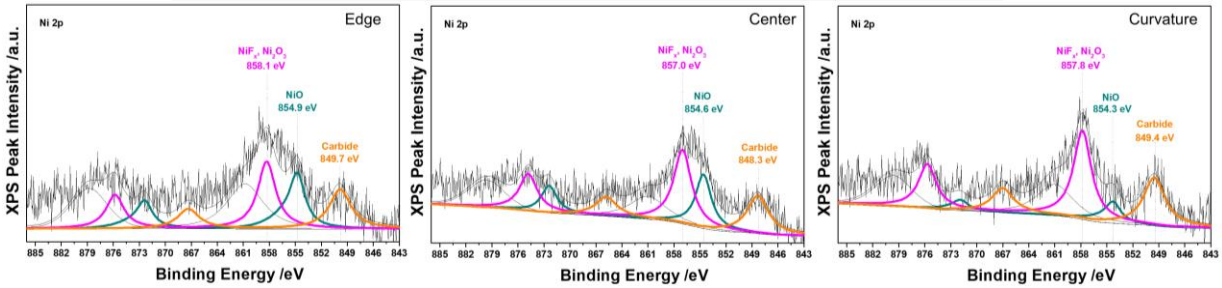

Figure S24 XPS Ni2p spectrum for Li_xC_6 and spatially distributed surface chemistry (e.g. edge, center, curvature) after post-mortem.

Percentages	Edge	Center	Curvature
Mass %	0	0.7	0
Atomic %	0	0.2	0

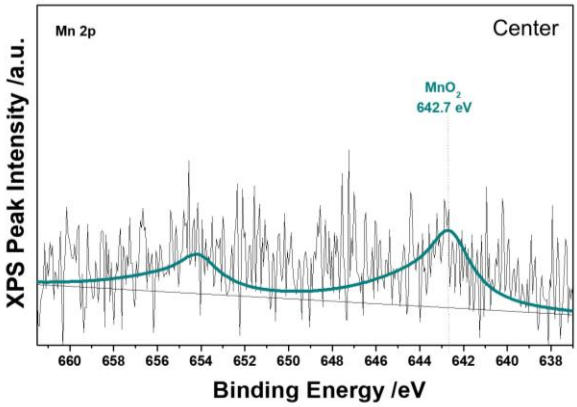

Figure S25 XPS Mn2p spectrum for Li_xC_6 and spatially distributed surface chemistry (e.g. edge, center, curvature) after post-mortem.

Percentages	Edge	Center	Curvature
Mass %	13.2	15.9	17.7
Atomic %	8.9	11.8	12.5

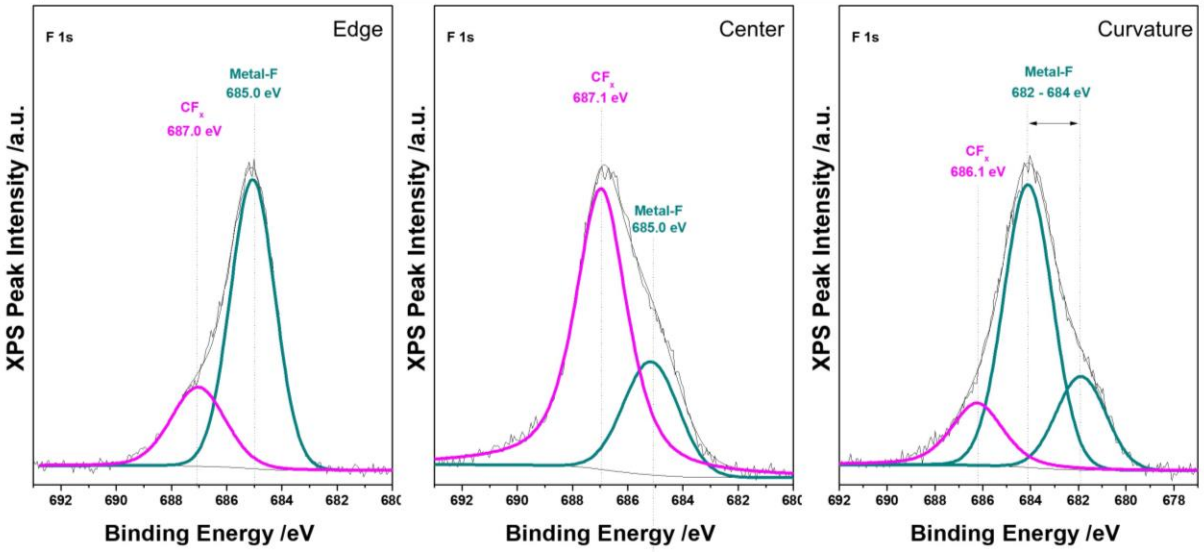

Figure S26 XPS F1s spectrum for Li_xC_6 and spatially distributed surface chemistry (e.g. edge, center, curvature) after post-mortem.

Percentages	Edge	Center	Curvature
Mass %	38.4	32.2	31.7
Atomic %	30.8	28.3	26.9

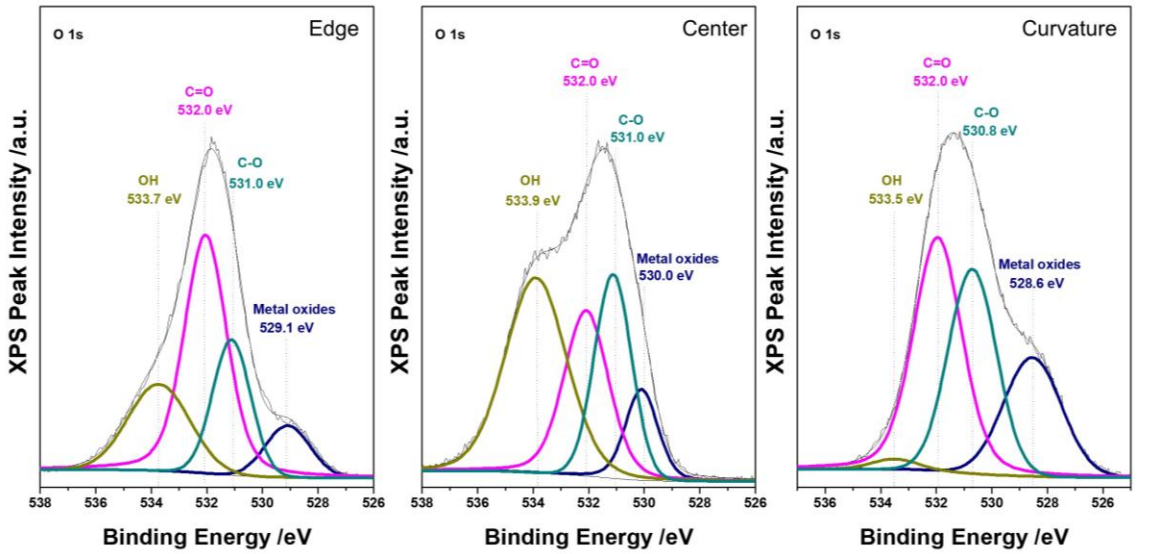

Figure S27 XPS O1s spectrum for Li_xC_6 and spatially distributed surface chemistry (e.g. edge, center, curvature) after post-mortem.

Percentages	Edge	Center	Curvature
Mass %	1.6	2.1	2.5
Atomic %	0.7	0.9	1.1

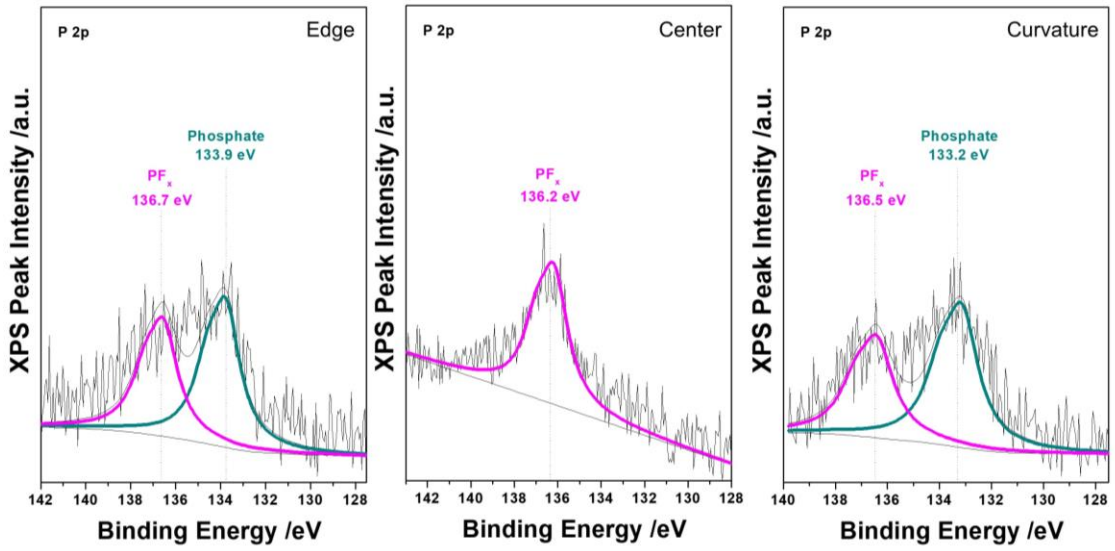

Figure S28 XPS P2p spectrum for Li_xC_6 and spatially distributed surface chemistry (e.g. edge, center, curvature) after post-mortem.

S8. Al_2O_3/Polyethylene Separator: SEM analysis and elemental mapping

Scanning electron microscopy (SEM) characterization of the separator was done to determine the architecture. Energy dispersive spectroscopy (EDS) elemental mapping of the separator indicates the presence of Al and C. Depositing alumina (Al_2O_3) on the anodic side of the separator is a common method to create a physical barrier that lessens the likelihood of Li^0 dendrite penetration, internal short circuit, and initiation of thermal runaway. Li^0 is too soft to cause penetration. Applied mechanical stress will force Li^0 to deform. Therefore, an alternative mechanism for internal short circuits is more likely. A combination of severe gassing and the significant increase in internal pressure can impart a force on low plastic deformation Li-corrosion products (e.g. Li-cabride and Ni-carbide. Hard materials like carbides can provide the structural rigidity to displace Al_2O_3 and the polymeric-components of the separator (~20microns or less due to mechanical indentation or pinching). In addition, the discovery of ripple-type electrode deformation behaviors during low temperature cycling, potentially enables puncturing at regions of delaminated Al_2O_3, which is caused by repetitive expansion/contraction.

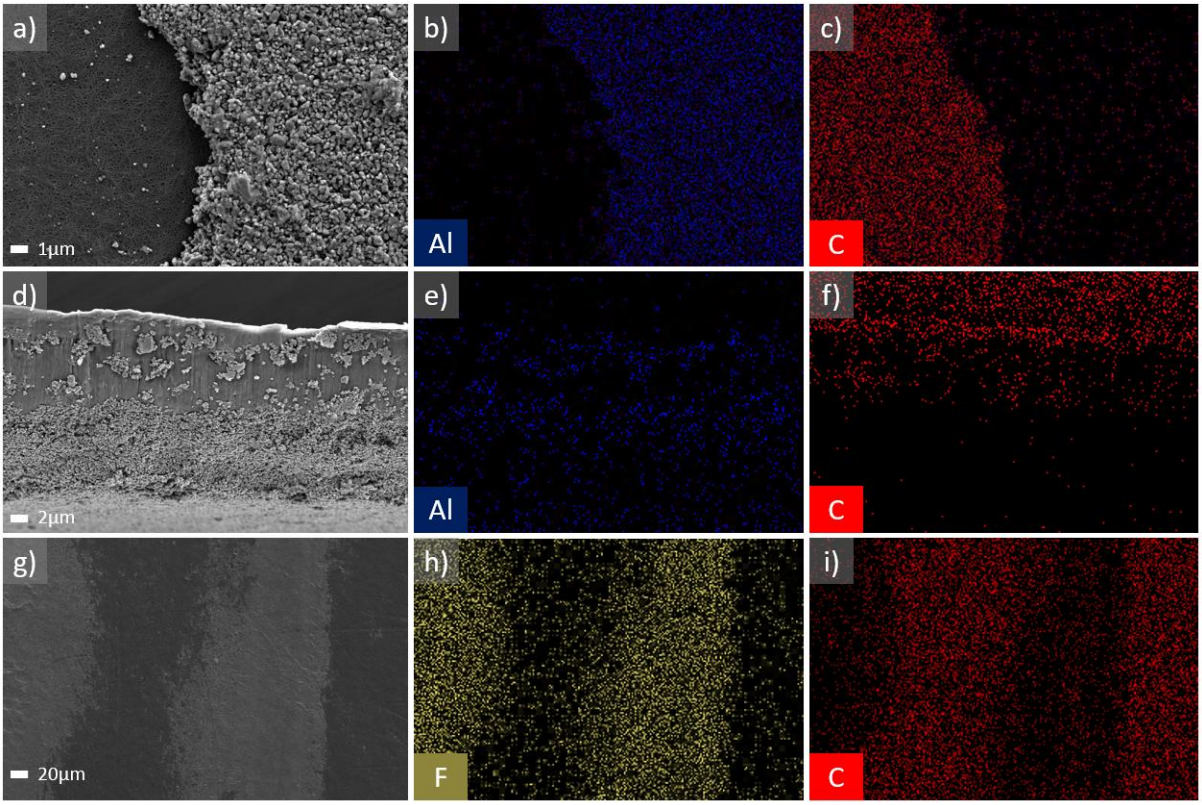

Figure S29. Field emission scanning electron microscope (FE-SEM) of the separator and EDS elemental mapping, which indicates the presence of Alumina (Al_2O_3) (indicated by blue) deposited on the anode side and a flame-retardant fluorinated polymer (indicated in yellow) on the cathode side for the suppression of Li^0 plating/dendrites and thermal processes.

References

1. Wang, Y., Nakamura, S., Tasaki, K. & Balbuena, P. B. Theoretical studies to understand surface chemistry on carbon anodes for lithium-ion batteries: How does vinylene carbonate play its role as an electrolyte additive? J. Am. Chem. Soc. **124**, 4408–4421 (2002).